**Jeomorfolojik Araştırmalar Dergisi**
Journal of Geomorphological Researches
© Jeomorfoloji Derneği www.dergipark.gov.tr/jader E - ISSN: 2667 - 4238

## Araştırma Makalesi / Research Article

# Lara Plajı'nda (Antalya, Türkiye) 1984–2025 Döneminde Kıyı Çizgisi Değişiminin Google Earth Engine ve DSAS ile Çok Zamanlı Analizi

# Multi-Temporal Analysis of Shoreline Change at Lara Beach (Antalya, Türkiye) from 1984 to 2025 Using Google Earth Engine and DSAS

**Ali ÜNVER**[a]

[a]Sorumlu Yazar / Corresponding Author
Bilecik Şeyh Edebali Üniversitesi, Lisansüstü Eğitim Enstitüsü, Coğrafya Bölümü, Bilecik, TÜRKİYE
aliunver3216@gmail.com https://orcid.org/0009-0002-5765-9132

Makale Tarihçesi
Geliş 8 Mayıs 2026
Kabul 4 Haziran 2026

Article History
Received: 8 May 2026
Accepted: 4 June 2026

Anahtar Kelimeler
Lara Plajı, Kıyı Çizgisi Değişimi, Google Earth Engine, DSAS, Uzaktan Algılama

Keywords
Lara Beach, Shoreline Change, Google Earth Engine, DSAS, Remote Sensing

Atıf Bilgisi / Citation Info
Ünver, A. (2026) Multi-Temporal Analysis of Shoreline Change at Lara Beach (Antalya, Türkiye) from 1984 to 2025 Using Google Earth Engine and DSAS, Jeomorfolojik Araştırmalar Dergisi / Journal of Geomorphological Researches, 2026 (17): 2

doi: 10.46453/jader.1947415

ÖZET

Bu çalışma, Antalya kıyısında yer alan Lara Plajı'nda 1984-2025 döneminde meydana gelen kıyı çizgisi değişimini, Google Earth Engine (GEE) tabanlı uzaktan algılama iş akışı ve Digital Shoreline Analysis System (DSAS) karşılaştırmasıyla incelemektedir. Çalışmanın temel amacı, kıyı çizgisindeki uzun dönemli değişimin yönünü, büyüklüğünü ve kıyı boyunca gösterdiği mekânsal farklılaşmayı ortaya koymaktır. Analizler, Landsat Collection 2 Level 2 Surface Reflectance görüntüleri kullanılarak 1984, 1990, 2000, 2010, 2015, 2020 ve 2025 yıllarını temsil eden yedi ana dönem üzerinden yürütülmüştür. Kıyı çizgileri, GEE ortamında oluşturulan mevsimsel medyan kompozitler ve Modifiye Normaleştirilmiş Su Fark İndisi (MNDWI) yaklaşımıyla çıkarılmış; kıyı değişimi, 100 m aralıklarla yerleştirilen 84 geçerli transekt boyunca Net Shoreline Movement (NSM), End Point Rate (EPR) ve Linear Regression Rate (LRR) metrikleri kullanılarak değerlendirilmiştir. Bulgular, Lara Plajı'nda uzun dönem ortalamasının negatif olduğunu, ancak bu sonucun kıyı boyunca tekdüze bir gerileme anlamına gelmediğini göstermektedir. GEE tabanlı sonuçlara göre ortalama NSM -0.69 m, ortalama EPR -0.02 m/yıl ve ortalama LRR -0.03 m/yıl olarak hesaplanmıştır. Geçerli 84 transektin 41'i erozyon, 43'ü ise birikim sınıfında yer almıştır. Bu dağılım, kıyı çizgisi gerilemesi ve birikim alanlarının aynı kıyı uzanımı boyunca birlikte bulunduğunu göstermektedir. Dönemsel sonuçlar, 1990 yılında kıyı çizgisinin deniz yönünde belirgin biçimde ilerlediğini; 1990-2000 ve 2000-2015 dönemlerinde gerilemenin daha baskın hale geldiğini; 2015 sonrasında ise bazı kesimlerde kısmi toparlanma yaşandığını ortaya koymaktadır. GEE ve DSAS karşılaştırmasında NSM için 0.838, EPR için 0.779 ve LRR için 0.733 düzeyinde korelasyon elde edilmiştir. Sonuç olarak bulgular, Lara Plajı'nın tek yönlü ve kesintisiz bir erozyon süreciyle açıklanamayacağını; erozyon ve birikimin kıyı boyunca birlikte görüldüğü, mekânsal olarak heterojen bir kıyı sistemi olduğunu göstermektedir.

ABSTRACT

This study examines shoreline change at Lara Beach on the Antalya coast of Türkiye over the 1984-2025 period by combining a Google Earth Engine (GEE)-based remote-sensing workflow with a comparison against Digital Shoreline Analysis System (DSAS) outputs. The aim is to identify the direction, magnitude, and alongshore variability of shoreline change. Landsat Collection 2 Level 2 Surface Reflectance imagery was used for seven primary epochs: 1984, 1990, 2000, 2010, 2015, 2020, and 2025. Shorelines were extracted from seasonal median composites using the Modified Normalized Difference Water Index (MNDWI), and shoreline change was evaluated along 84 valid shore-normal transects using Net Shoreline Movement (NSM), End Point Rate (EPR), and Linear Regression Rate (LRR). The results indicate a negative long-term mean for Lara Beach, but not a uniform pattern of shoreline retreat. In the GEE-based analysis, mean NSM, EPR, and LRR were -0.69 m, -0.02 m/yr, and -0.03 m/yr, respectively. Of the 84 valid transects, 41 were classified as erosional and 43 as accretional, showing that retreating and advancing parts of the shoreline coexist within the same beach system. The temporal pattern is also mixed: the shoreline advanced in 1990 relative to 1984, retreated more clearly between 1990 and 2015, and then showed partial recovery after 2015. The comparison between GEE and DSAS yielded strong to substantial agreement, with correlation coefficients of 0.838 for NSM, 0.779 for EPR, and 0.733 for LRR. These results support a site-specific interpretation of Lara Beach as a spatially variable sandy coast rather than as a uniformly erosional shoreline.

# 1. INTRODUCTION

## 1.1. Research background and literature review

Coastal zones are dynamic geomorphic environments in which waves, currents, sediment supply, sea-level variability, wind action, episodic high-energy events, and human intervention act together rather than separately. For that reason, shoreline position is widely used as an indicator of coastal change, but it should be interpreted with attention to the local sediment budget, shoreline proxy, and geomorphological setting of the investigated coast (Carter, 1988; Komar, 1998; Masselink & Hughes, 2003; Boak & Turner, 2005). Recent shoreline-change studies increasingly combine multi-temporal satellite imagery, GIS-based transect analysis, and explicit uncertainty discussion to avoid reducing complex coastal behaviour to a single mean rate (Himmelstoss et al., 2021; Abd-Elhamid et al., 2023; Darwish & Smith, 2023; Molina et al., 2024).

This point is especially important on sandy Mediterranean coasts. Such coasts may be microtidal in character, but they can still respond sharply to storm waves, river-mouth sediment supply, alongshore transport, aeolian reworking, dam-related reductions in sediment delivery, and coastal structures. Studies from the eastern Mediterranean show that deltaic and sandy coasts may pass through alternating phases of progradation, retreat, and localized rebuilding under both natural and anthropogenic controls (Özpolat & Demir, 2019; Özpolat et al., 2021; Kuleli, 2010; Gümüş, 2024). Thus, a visually continuous sandy beach should not automatically be treated as a geomorphologically uniform unit.

The growing availability of long Landsat archives has made this type of analysis more reproducible. GEE is particularly useful because it allows multi-decadal image archives to be filtered, masked, composited, and analysed in the cloud without downloading each scene separately (Gorelick et al., 2017). Several spectral water indices can be used for land-water separation, including NDWI, MNDWI and AWEI-type approaches. MNDWI was selected here because the green-SWIR1 contrast generally improves the separation of open water from built-up, vegetated, and moist non-water surfaces in mixed coastal settings (Xu, 2006). The choice does not imply that MNDWI is universally superior in every beach environment; it was adopted as a consistent shoreline proxy for the Landsat-based, multi-epoch comparison used in this study.

For shoreline-change assessment, transect-based approaches remain standard in coastal geomorphology. DSAS provides a widely used framework for calculating metrics such as NSM, EPR, LRR and SCE (Thieler et al., 2009; Himmelstoss et al., 2021). In Türkiye, DSAS and related remote-sensing approaches have been applied to a wide range of coastal settings, including the Göksu, Kızılırmak, Yeşilırmak, Meriç, Bakırçay and Küçük Menderes deltas, the Gulf of İzmit, Riva, Beymelek, Dalaman, Karaburun-Kumköy and harbour-influenced sandy coasts around Samsun (Kılar & Çiçek, 2018; Ataol et al., 2019; Kale et al., 2019; Ciritci & Türk, 2020; Akdeniz & İnam, 2023; Kılar, 2023; Öztürk & Uzun, 2023; Uzun, 2023; Kılar & Aydın, 2024; Kılar & Kömüşcü, 2024; Öztürk & Maraş, 2024; Öztürk & Sesli, 2015; Öztürk et al., 2015; Ateş et al., 2024; Uzun, 2024; Uzun, 2025). These studies are not used here to validate the Lara results; they show that Turkish coasts often require site-specific, transect-based interpretation because erosion and accumulation may be concentrated in different parts of the same coastal system.

Despite the geomorphological and socio-economic importance of the Antalya coast, long-term and spatially explicit shoreline-change studies focused specifically on Lara Beach remain limited. This gap matters because Lara is not only a tourist beach; it is also a sandy coastal system where foreshore change, backshore constraint, stream/channel-mouth conditions, and human-modified margins can influence how the shoreline responds through time. The present study therefore focuses on Lara's own metrics, maps, and field observations, and uses wider literature only to

frame the methodological and geomorphological discussion.

### 1.2. Aim and scope of the study

This study examines shoreline change along Lara Beach using multi-temporal Landsat imagery, a GEE-based shoreline extraction workflow, and a transect-based analytical framework for the 1984-2025 period. The core rate calculations are based on seven primary shoreline epochs, while the annual GEE image archive was also reviewed to understand the continuity of image support and the direction of mean shoreline shifts through time. A supplementary 2023-2026 composite was prepared only to support present-day visualization and was not included in the long-term trend calculations.

The objectives are to reconstruct the main shoreline positions between 1984 and 2025; quantify long-term and period-specific shoreline change using NSM, EPR and LRR; identify the alongshore distribution of erosion, accretion and near-stability; and compare the GEE-derived results with DSAS outputs. The paper therefore aims to produce a site-specific geomorphological interpretation of Lara Beach, not only a technical comparison between two software environments.

### 1.3. Study area

#### 1.3.1. Geographic setting

The study area is located along Lara Beach on the eastern coast of Antalya, in southwestern Türkiye, on the Mediterranean littoral. As shown in Figure 1, the investigated sector lies east of Antalya's urban core, where sandy beach morphology coincides with intensive tourism-related land use and coastal infrastructure.

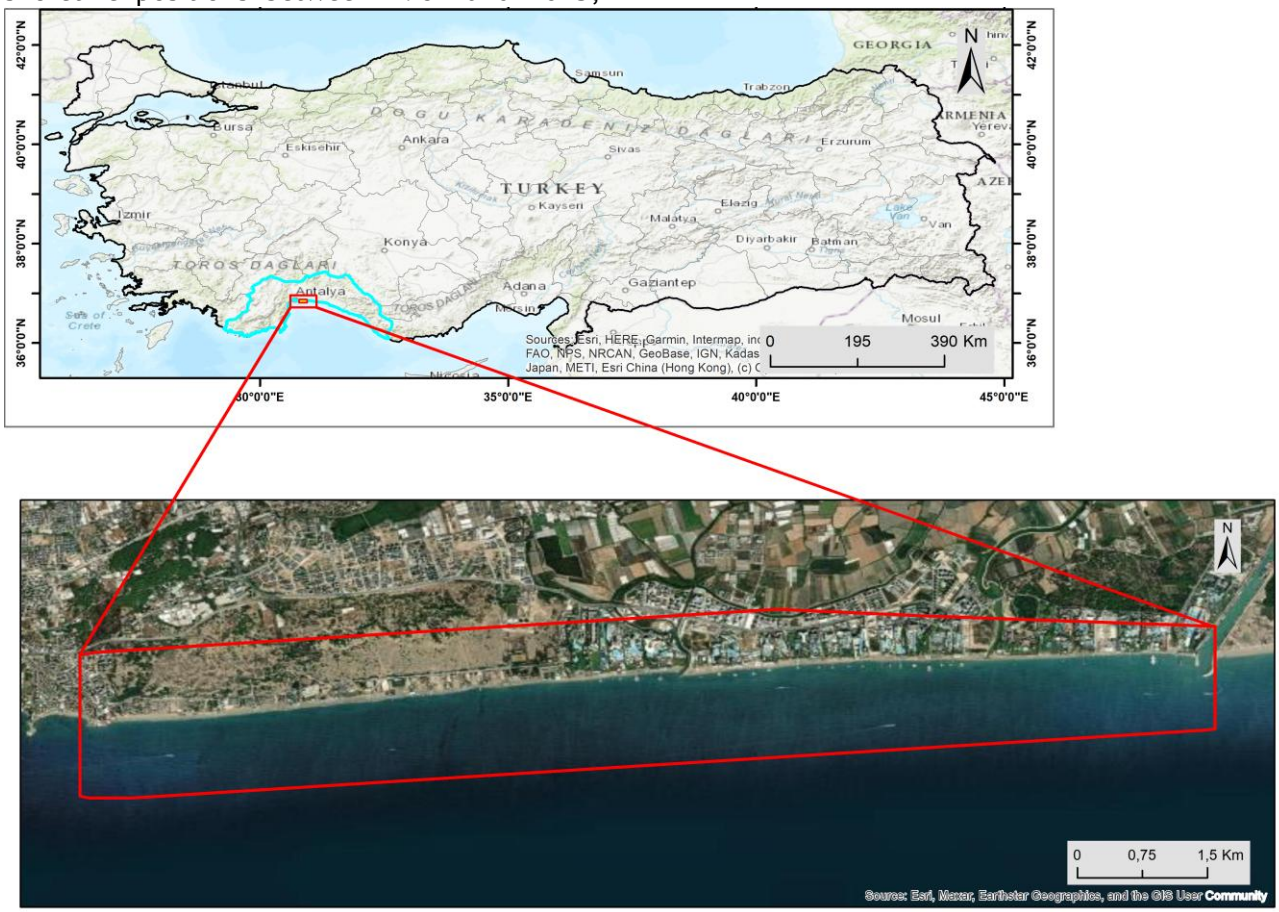


**Figure 1.** Location of the Lara Beach study area on the eastern Mediterranean coast of Antalya, southwestern Türkiye. / **Şekil 1.** Lara Plajı çalışma alanının güneybatı Türkiye'de, Antalya'nın doğu Akdeniz kıyısındaki konumu.

Lara Beach forms part of the broader Antalya coastal system, one of the most intensively used littoral environments in southern Türkiye. The analysed reach is a broadly straight sandy shoreline approximately 10.12 km long. This planform is suitable for transect-based analysis because it allows regular shore-normal sampling, but it should not be read as evidence of uniform geomorphological behaviour. Even along a straight sandy shoreline, local

differences in sediment storage, stream/channel-mouth influence, backshore condition, and human intervention can produce different shoreline responses over short alongshore distances.

The wider coastal setting includes beach surfaces, tourism-oriented land use, transport and service infrastructure, and low-relief coastal terrain. These characteristics make Lara Beach a relevant site for shoreline-change analysis, as it combines the morphodynamic sensitivity of a sandy Mediterranean coast with sustained anthropogenic pressure. In such settings, shoreline adjustment may reflect not only hydrodynamic forcing, but also the indirect effects of backshore constraint and land-use intensity.

### 1.3.2. Geomorphological characteristics of Lara Beach

Geomorphologically, Lara Beach is treated as a wave-dominated sandy beach system composed of interacting nearshore, foreshore and backshore zones. The shoreline proxy used in this study represents the land-water boundary extracted from Landsat-based MNDWI composites; it should therefore be interpreted as a consistent remote-sensing shoreline indicator, not as a direct survey of every morphological sub-zone. The field observations were used to relate mapped shoreline behaviour to present-day foreshore width, berm or upper-beach expression, sediment accumulation and visible anthropogenic modification.

Although the planform of Lara Beach is broadly linear, the beach is not assumed to behave as a single homogeneous geomorphic unit. Differences in foreshore width, backshore constraint, local sediment storage, channel-mouth morphology, and anthropogenic boundaries may lead neighbouring parts of the same beach to show shoreline retreat, near-stability, or seaward advance during the same analysis period.

This interpretation is also relevant in the Mediterranean context, where average hydrodynamic conditions may be moderate, yet episodic high-energy events can still produce marked local change. Under such conditions, reach-scale averages may conceal substantial transect-level variability. Accordingly, Lara Beach is treated here as a spatially heterogeneous littoral system in which neighbouring sectors may display retreat, relative stability, or seaward advance within the same overall coastal reach.

The geomorphological framing adopted in this study therefore emphasizes shoreline variability rather than assuming uniform coastal response. This perspective provides the basis for the transect-based analysis presented in the following sections and guides the interpretation of long-term shoreline-change metrics.

## 2. MATERIALS AND METHODS

### 2.1. Data sources and temporal framework

All shoreline analyses were carried out in Google Earth Engine (GEE), a cloud-based geospatial platform widely used for processing large remote sensing archives and building reproducible spatial workflows (Gorelick et al., 2017). The temporal framework of the study was established using Landsat Collection 2 Level 2 Surface Reflectance imagery, allowing shoreline behaviour at Lara Beach to be examined over the period 1984-2025. To reduce seasonal inconsistency and improve comparability among observation years, the primary shoreline epochs were restricted to the summer months (June-September).

As summarized in Table 1, the long-term quantitative analysis was based on seven primary shoreline epochs: 1984, 1990, 2000, 2010, 2015, 2020 and 2025. All primary epochs were restricted to June-September imagery in order to reduce seasonal inconsistency and to keep the shoreline proxy comparable among years. The GEE environment also allowed the annual image archive to be inspected without downloading individual scenes; however, the main NSM, EPR, LRR and GEE-DSAS comparison statistics were kept tied to the seven primary epochs so that the rate calculations remained transparent and directly comparable with DSAS. A separate multi-season design, for example April-July-October comparisons, would be valuable for seasonal process interpretation, but it was beyond the defined scope of the present multi-decadal analysis.

Table 2 summarizes the principal analytical settings. The analysed shoreline reach extends

for 10.12 km, while the landward baseline used for shoreline-distance measurements is 10.09 km long. The baseline was placed on the land side of the beach and approximately parallel to the general shoreline alignment. Shoreline change was evaluated along 84 valid shore-normal transects spaced at 100 m intervals across the consistently mappable part of the study reach. A denser 30-50 m transect grid could provide finer local detail, but it would also require a full reprocessing of all GEE and DSAS outputs. Therefore, the existing 100 m framework was retained and its limitation was stated explicitly, because all tables, figures and cross-platform comparisons were produced from the same internally consistent transect network.

**Table 1.** Data inventory and image support used for shoreline extraction and temporal comparison. / **Tablo 1.** Kıyı çizgisi çıkarımı ve zamansal karşılaştırma için kullanılan veri envanteri ve görüntü desteği.

| Epoch | Start date | End date | Image count | Role | Dataset |
|---|---|---|---|---|---|
| 1984 | 1984-06-01 | 1984-09-30 | 5 | Primary epoch | Landsat Collection 2 Level 2 SR |
| 1990 | 1990-06-01 | 1990-09-30 | 6 | Primary epoch | Landsat Collection 2 Level 2 SR |
| 2000 | 2000-06-01 | 2000-09-30 | 17 | Primary epoch | Landsat Collection 2 Level 2 SR |
| 2010 | 2010-06-01 | 2010-09-30 | 8 | Primary epoch | Landsat Collection 2 Level 2 SR |
| 2015 | 2015-06-01 | 2015-09-30 | 23 | Primary epoch | Landsat Collection 2 Level 2 SR |
| 2020 | 2020-06-01 | 2020-09-30 | 24 | Primary epoch | Landsat Collection 2 Level 2 SR |
| 2025 | 2025-06-01 | 2025-09-30 | 30 | Primary epoch | Landsat Collection 2 Level 2 SR |
| Recent | 2023-01-01 | 2026-04-18 | 323 | Supplementary recent composite | Landsat Collection 2 Level 2 SR |

**Table 2.** Analytical settings and methodological parameters used in the GEE-based shoreline-change workflow. / **Tablo 2.** GEE tabanlı kıyı çizgisi değişimi iş akışında kullanılan analitik ayarlar ve yöntemsel parametreler.

| Item | Value |
|---|---|
| Study reach | Lara Beach, Antalya |
| Primary analysis period | 1984-2025 |
| Supplementary recent composite | 2023-01-01 to 2026-04-18 |
| Straight shoreline span (km) | 10.12 |
| Baseline length (km) | 10.09 |
| Transect count | 84 |
| Transect spacing (m) | 100 |
| Transect length (m) | 1100 |
| Shoreline search band (m) | 550 |
| Shoreline snap buffer (m) | 45 |
| MNDWI threshold | 0.00 |
| Satellite calibration approach | Common green-SWIR1 MNDWI on harmonized Landsat C2 L2 SR |
| Trend metrics | NSM, EPR, LRR |

### 2.2. Analytical framework and shoreline extraction

The overall spatial design of the analysis is presented in Figure 2. The study geometry was first established by defining a shoreline-oriented analysis axis between the western and eastern endpoints of the investigated coastal reach. Based on this axis, an area of interest (AOI) was delineated to encompass not only the active beach zone, but also adjacent coastal margins that could influence shoreline extraction and interpretation. An alongshore analysis corridor was then constructed to constrain the extraction process to the target beach sector while preserving the locally modified eastern boundary, where anthropogenic structures and stream-mouth-adjacent conditions may influence shoreline behaviour.


**Figure 2.** Study area and analysis framework showing the area of interest (AOI), shoreline analysis corridor, baseline, segment endpoints, and shore-normal transects used for shoreline-change calculations. / **Şekil 2.** Kıyı çizgisi değişim hesaplamalarında kullanılan ilgi alanı (AOI), analiz koridoru, başlangıç çizgisi, segment uç noktaları ve kıyıya dik transektleri gösteren çalışma alanı ve analiz çerçevesi

For image preprocessing, Landsat 5 TM and Landsat 7 ETM+ scenes were harmonized using the green and SWIR1 bands represented by SR_B2 and SR_B5, whereas Landsat 8 OLI and Landsat 9 OLI-2 scenes were processed using SR_B3 and SR_B6. In all cases, surface reflectance values were converted according to the Landsat Collection 2 Level 2 scaling factors implemented in the workflow. To improve spectral reliability prior to shoreline extraction, only clear and non-saturated pixels were retained using the QA_PIXEL and QA_RADSAT quality masks. This masking step reduced the influence of cloud, cloud shadow, snow, and radiometric saturation on the resulting shoreline vectors.

For each target epoch, the filtered Landsat scenes were composited into a median seasonal image clipped to the AOI. Shoreline extraction was based on the Modified Normalized Difference Water Index (MNDWI):

$$MNDWI = \frac{Green - SWIR1}{Green + SWIR1}$$

MNDWI was selected after considering the broader family of water indices used in shoreline mapping, including NDWI and AWEI-type approaches. For Lara Beach, the MNDWI formulation was preferred because the use of SWIR1 helps reduce spectral confusion between open water and non-water surfaces such as built-up land, moist sand, vegetation and shaded coastal margins. A fixed threshold of 0.00 was adopted as a standardizing operational choice across sensors and epochs. This threshold produced a coherent first-order land-water separation in the study area, but it is not presented as a universal threshold for all coastal environments. Residual threshold sensitivity, wet-sand response and water turbidity are therefore discussed as sources of positional uncertainty.

The refined water mask was subsequently converted into vector polygons. To isolate the marine water body from inland or disconnected water patches, the polygon intersecting an offshore control point was retained as the target sea polygon. The shoreline itself was

represented by the exterior boundary of that polygon. In the final step, the extracted shoreline was clipped using both the shoreline search band and the alongshore analysis corridor so that the resulting shoreline vector corresponded closely to the intended beach reach rather than to unrelated water boundaries elsewhere in the AOI. This procedure follows the broader methodological principle that shoreline extraction should rely on a clearly defined shoreline proxy within a spatially constrained analytical domain (Boak & Turner, 2005).

### 2.3. Baseline construction, transect geometry, and shoreline distances

A landward baseline, positioned approximately parallel to the general shoreline alignment, was manually defined to provide a stable reference for transect-based shoreline analysis. From this land-side baseline, 84 valid shore-normal transects were generated at 100 m intervals along the consistently analyzable part of the study reach, and each transect extended 1100 m seaward. The generated transect network was clipped and filtered so that only transects intersecting valid shoreline segments in the defined search domain were retained for the final calculations.

To ensure that shoreline positions were measured within the intended coastal domain, a shoreline search band of 550 m was applied around the baseline. A shoreline snap buffer of 45 m was also used during distance extraction so that each transect could be linked to the most relevant nearby shoreline segment. These settings helped reduce the influence of unrelated shoreline fragments and improved the consistency of shoreline-distance measurements across the study area.

For each transect, shoreline position was expressed as the distance between the landward transect origin and the shoreline location identified within the predefined search domain. In practical terms, seven primary shoreline vectors were extracted for the 1984-2025 analysis, and each valid transect was used to measure the shoreline position for those epochs. Transects with missing or ambiguous shoreline intersections were excluded from the relevant rate calculation. The extracted positions are therefore treated as standardized analytical measurements of a Landsat-derived shoreline proxy rather than field-surveyed shoreline points.

Given the broadly linear planform of Lara Beach, the representative shoreline position measured within each transect search domain was considered suitable for standardized multi-temporal comparison in the constrained study area. The resulting shoreline distances are therefore interpreted as consistent analytical measurements rather than direct field measurements. Transects for which no valid shoreline segment could be identified were excluded from subsequent rate calculations through a missing-data filter.

### 2.4. Shoreline-change metrics

Long-term shoreline change was quantified using three complementary transect-based metrics: Net Shoreline Movement (NSM), End Point Rate (EPR), and Linear Regression Rate (LRR). NSM was used because it directly expresses the net displacement between the first and last primary shoreline; EPR converts this displacement into an annualized endpoint rate; and LRR uses the full multi-epoch sequence to estimate the long-term trend. Shoreline Change Envelope (SCE) was also calculated in the DSAS comparison as a supporting shoreline-mobility metric. Unlike NSM, EPR and LRR, SCE does not indicate the direction or annual rate of shoreline change; however, it is important because it expresses the maximum distance between the most landward and most seaward shoreline positions along each transect. Therefore, SCE was not used as the main directional trend indicator in this study, but it was retained to characterize the magnitude of shoreline mobility and to support the interpretation of potentially sensitive sectors for coastal management.

NSM was calculated for each transect as the difference between the shoreline distance measured for the latest primary epoch and that measured for the earliest primary epoch:

$$NSM = D_{2025} - D_{1984}$$

where D represents shoreline distance measured from the fixed baseline. Positive NSM values indicate seaward shoreline movement and thus accretion, whereas negative values

indicate landward movement and therefore erosion.

EPR was calculated by dividing net shoreline movement by the elapsed time between the first and last primary shoreline dates:

$$EPR = \frac{D_{2025} - D_{1984}}{2025 - 1984}$$

This metric provides an annualized rate of shoreline change based solely on the endpoint shorelines. Because it relies only on the first and last observations, EPR is straightforward to interpret and useful for summarizing the overall long-term tendency.

LRR was derived by applying ordinary least squares regression to shoreline distance as a function of year across all valid primary epochs:

$$LRR = \beta_1$$

where β_1 is the slope of the fitted regression line. Unlike EPR, LRR incorporates the full multi-epoch shoreline record rather than relying only on the endpoints. It is therefore particularly informative where shoreline behaviour is non-monotonic and intermediate phases of retreat and recovery occur within the study period.

In addition to these long-term metrics, period-specific NSM and EPR values were also calculated for consecutive primary epochs, namely 1984–1990, 1990–2000, 2000–2010, 2010–2015, 2015–2020, and 2020–2025. This made it possible to assess whether shoreline change at Lara Beach followed a consistent long-term direction or alternated between retreat and recovery over successive sub-periods. By combining endpoint-based, regression-based, and interval-based measures, the analysis was designed to capture both the overall shoreline tendency and its temporal variability along the study reach.

### 2.5. DSAS-based comparison and statistical evaluation

To assess methodological consistency, shoreline-change metrics derived from the Google Earth Engine workflow were compared with outputs from the U.S. Geological Survey Digital Shoreline Analysis System (DSAS), a widely used tool for transect-based shoreline-change analysis (Thieler et al., 2009; Himmelstoss et al., 2021). The DSAS dataset included transect-level NSM, EPR, and LRR values, while SCE was retained as an additional indicator of shoreline variability. The comparison was used to evaluate whether the GEE-based workflow reproduced the broader spatial and statistical shoreline-change pattern obtained from an established analytical framework.

Matched shoreline-change values from the two analytical environments were compared on a transect-by-transect basis. For each metric, the evaluation included the Pearson correlation coefficient (r), mean absolute difference, median absolute difference, maximum absolute difference, and mean directional bias, expressed as DSAS minus GEE. These statistics were used to assess both the level of agreement and the magnitude of any systematic offset between the two methods.

This step was important because shoreline extraction, intersection handling, and distance calculation may differ according to the analytical platform, shoreline representation, and treatment of local shoreline geometry. Rather than assuming exact numerical equivalence between GEE and DSAS, the analysis tested whether both methods converged on the same general interpretation of long-term shoreline behaviour at Lara Beach. In this sense, the cross-platform comparison served as a robustness check for the overall methodological framework.

The DSAS summary metrics were also retained to support interpretation of long-term shoreline variability across the matched transects. The quantitative reliability of the GEE-DSAS comparison was evaluated through Pearson correlation, mean absolute difference, median absolute difference, maximum absolute difference and directional bias. Direct comparison was made only for 66 transects that produced valid one-to-one results in both workflows, while unmatched or invalid intersections were excluded to avoid forcing artificial correspondence between the two datasets.

### 2.6. Methodological considerations

Although the workflow was designed to maximize internal consistency, the Landsat-derived shoreline positions inevitably contain residual uncertainty. This uncertainty may arise from 30 m pixel size, image-to-image georegistration, threshold-dependent land-

water separation, seasonal compositing, wet-sand reflectance, swash-zone conditions, water turbidity and the distinction between an instantaneous waterline and a remotely sensed shoreline proxy (Crowell et al., 1991; Boak & Turner, 2005). For this reason, the results are interpreted at the level of first-order shoreline tendency and alongshore pattern rather than as exact sub-pixel displacement for individual dates.

Several methodological choices were adopted to reduce these effects. The primary shoreline epochs were restricted to the summer season to improve inter-epoch comparability, and all Landsat inputs were processed within a harmonized green-SWIR1 MNDWI framework to maintain consistent spectral logic across sensors (Xu, 2006). Median compositing was used to suppress scene-specific noise, while the fixed threshold, spatially constrained shoreline corridor, snap buffer, and stable transect geometry helped maintain consistency throughout the time series.

A full quantitative uncertainty budget and dedicated multi-threshold sensitivity experiment were not implemented within the scope of this study. Accordingly, the results are interpreted at the level of first-order shoreline tendencies and alongshore spatial variability, rather than as exact sub-pixel displacements for individual transects or dates. This limitation is particularly relevant where mean changes remain close to zero, since weak aggregate shifts may fall within the positional uncertainty inherent in medium-resolution shoreline mapping. Within this scope, however, the workflow provides a reproducible basis for distinguishing clearer erosional and accretional sectors from near-stable portions of the shoreline and for comparing the overall shoreline signal with DSAS-derived results (Thieler et al., 2009; Himmelstoss et al., 2021).

### 2.7. Field observations and photographic documentation

Field observations and photographic documentation were used to provide present-day geomorphological context for the shoreline-change patterns derived from remote sensing and DSAS. They were not used as independent validation of historical shoreline positions. The field component instead helped describe current foreshore width, berm or upper-beach form, sediment accumulation, backshore condition, stream/channel-mouth morphology and visible anthropogenic influence in representative parts of the study reach.

During the field visit, representative parts of the Lara Beach study reach were photographed and described through rapid geomorphological observation. Attention was given to the continuity of the sandy foreshore, the swash zone, upper-beach and backshore conditions, sediment texture, visible depositional features, artificial coastal margins and signs of local sediment handling. These observations were used as present-day geomorphological context only; they do not constitute repeated field measurements, sediment-budget analysis or direct validation of the historical GEE/DSAS shoreline positions.

Accordingly, broad sandy beach sectors, the stream/channel-mouth area and adjacent modified margins were used only to interpret the contemporary setting of the mapped shoreline pattern. Stockpiled sediment and machinery are treated cautiously as evidence of local sediment handling or possible reworking, not as proof of systematic beach nourishment.

Overall, the field component links the multi-decadal shoreline-change metrics with present-day indicators of coastal form, sediment storage, channel-mouth influence, and anthropogenic modification.

## 3. RESULTS

### 3.1. Temporal distribution of imagery and reconstructed shoreline positions

The temporal distribution of the Landsat archive used for shoreline reconstruction is presented in Figure 3. Image availability increased substantially through time, rising from 5 scenes in 1984 and 6 scenes in 1990 to 30 scenes in 2025, whereas the supplementary recent composite was supported by 323 scenes. The larger image pool available for the later years likely increased the robustness of the seasonal composites by reducing the influence of individual scenes on the final extracted shoreline position.

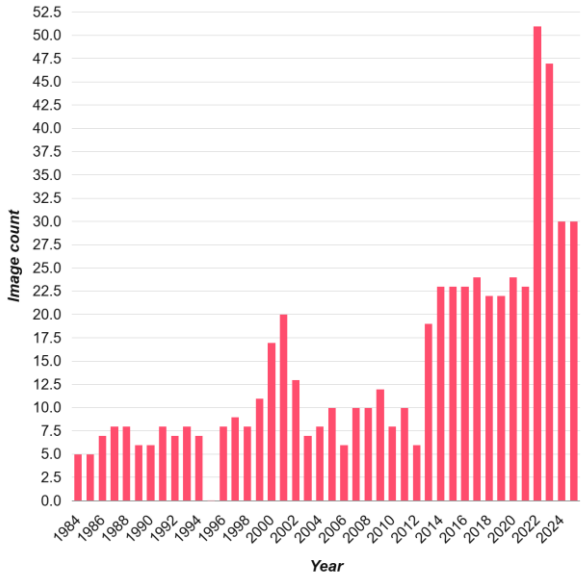


**Figure 3.** Annual image support used for shoreline reconstruction across the primary epochs and the supplementary recent composite. / **Şekil 3.** Birincil dönemler ve destekleyici güncel bileşik için kıyı çizgisi yeniden oluşturulmasında kullanılan yıllık görüntü desteği.

The reconstructed shoreline positions for the seven primary epochs are shown in Figure 4. In planform, the shoreline series indicates that Lara Beach retained its broadly linear coastal configuration throughout the 1984–2025 period, although several sectors experienced alternating landward and seaward displacements. This pattern suggests that shoreline evolution along the study reach did not follow a simple one-directional trend. Instead, shoreline mobility varied across both space and time, reflecting a combination of retreat, local stability, and partial re-advance.

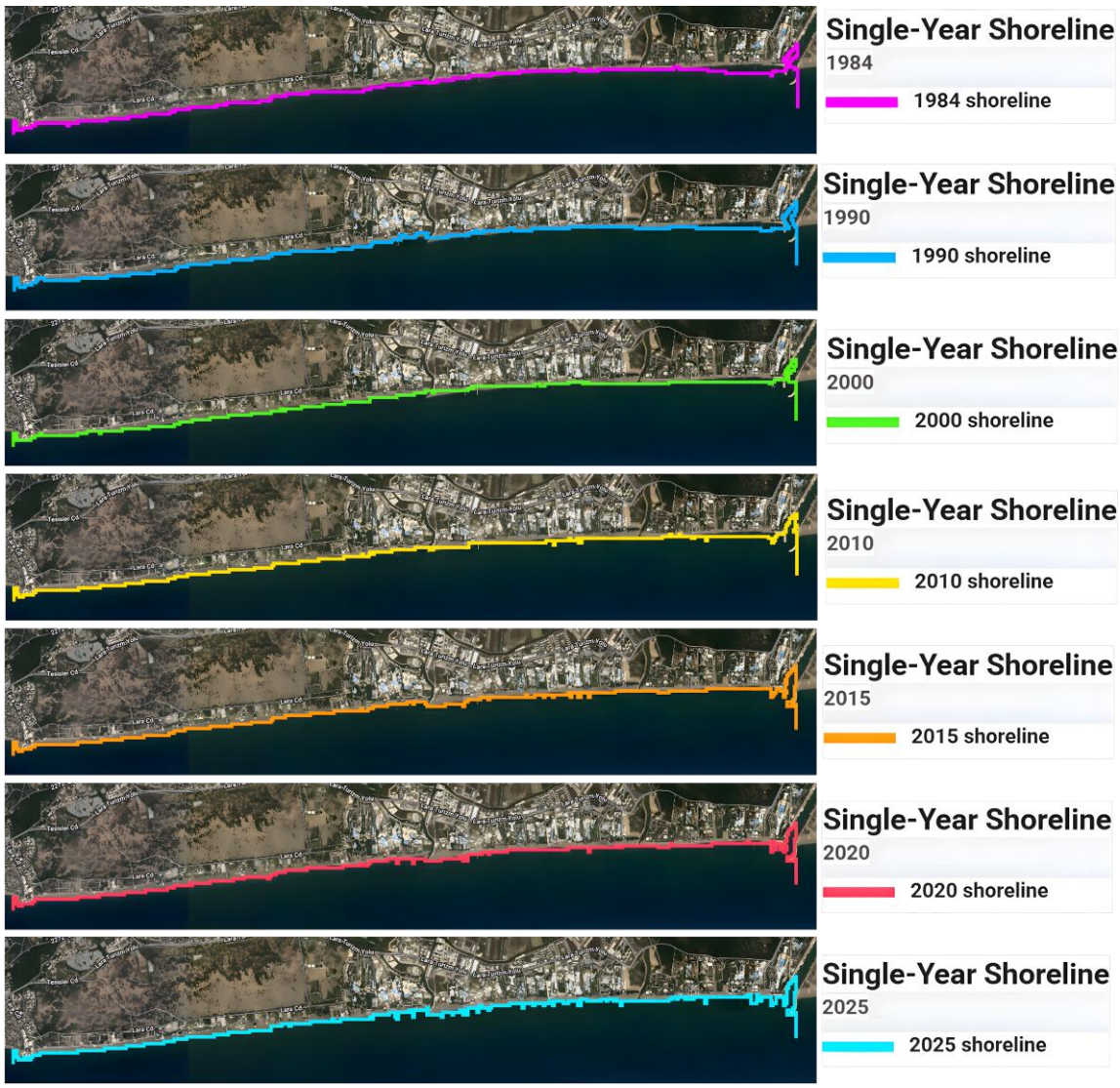


**Figure 4.** Reconstructed shoreline positions for 1984, 1990, 2000, 2010, 2015, 2020, and 2025. / **Şekil 4.** 1984, 1990, 2000, 2010, 2015, 2020 ve 2025 yılları için yeniden oluşturulan kıyı çizgisi konumları.


**Figure 5.** Comparison of the 1984 and 2025 reference shorelines along the Lara Beach study reach. / **Şekil 5.** Lara Plajı çalışma alanı boyunca 1984 ve 2025 referans kıyı çizgilerinin karşılaştırılması.

A direct comparison between the earliest and latest primary shorelines is presented in Figure 5. Although the 1984 and 2025 shoreline envelopes broadly overlap in planform, the comparison reveals localized sectors of both retreat and advance. This indicates that long-term shoreline behaviour at Lara Beach is more appropriately described in terms of alongshore heterogeneity than uniform shoreline translation across the entire study reach.

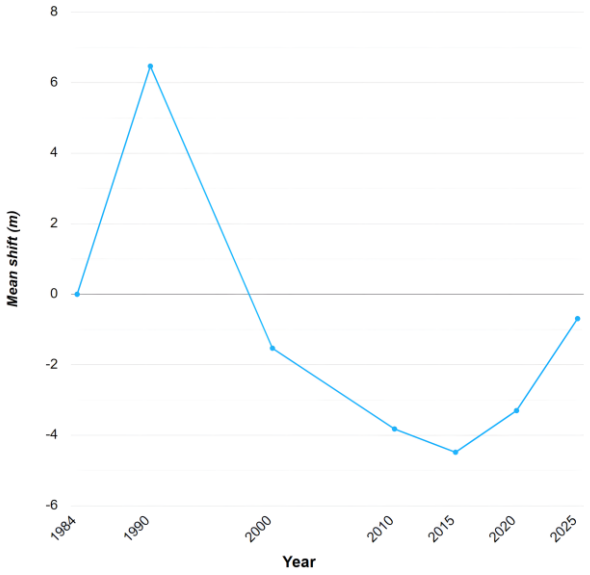


**Figure 6.** Mean shoreline change relative to the 1984 baseline condition. Positive values indicate seaward shoreline advance, whereas negative values indicate shoreline retreat. / **Şekil 6.** 1984 başlangıç durumuna göre ortalama kıyı çizgisi değişimi. Pozitif değerler kıyı çizgisinin deniz yönünde ilerlediğini, negatif değerler ise kara yönünde gerilediğini göstermektedir.

The temporal evolution of mean shoreline shift relative to the 1984 baseline condition is shown in Figure 6, and the corresponding descriptive statistics are summarized in Table 3. The shoreline first shifted seaward in 1990 by +6.47 m, then moved landward relative to 1984 in 2000 (−1.53 m), 2010 (−3.82 m), and 2015 (−4.48 m). A partial recovery followed in 2020 (−3.30 m) and 2025 (−0.69 m), indicating that long-term shoreline behaviour was oscillatory rather than consistently directional. The lowest relative mean position occurred in 2015. By 2025, the shoreline had nearly returned to its 1984 mean position, although a slight negative offset remained.

**Table 3.** Yearly shoreline summary for the primary shoreline epochs. / **Tablo 3.** Birincil kıyı çizgisi dönemleri için yıllık kıyı çizgisi özeti.

| Epoch | Image count | Mean shoreline distance (m) | Median shoreline distance (m) | Mean shift from 1984 (m) |
|---|---|---|---|---|
| 1984 | 5 | 152.22 | 113.93 | 0.00 |
| 1990 | 6 | 158.69 | 127.16 | 6.47 |
| 2000 | 17 | 150.69 | 114.05 | -1.53 |
| 2010 | 8 | 148.40 | 104.25 | -3.82 |
| 2015 | 23 | 147.74 | 91.59 | -4.48 |
| 2020 | 24 | 148.92 | 102.38 | -3.30 |
| 2025 | 30 | 151.52 | 100.63 | -0.69 |

The central tendency of shoreline position through time is further illustrated in Figure 7, which compares mean and median shoreline distances. Mean shoreline distance from the baseline was 152.22 m in 1984, increased to 158.69 m in 1990, and then declined to 150.69 m in 2000, 148.40 m in 2010, 147.74 m in 2015,

148.92 m in 2020, and 151.52 m in 2025. Median shoreline distance followed a somewhat different trajectory, reaching 127.16 m in 1990 before declining to 91.59 m in 2015 and then recovering slightly during the later epochs. Taken together, these values indicate alternating phases of retreat and partial re-advance rather than a single persistent shift in one direction.

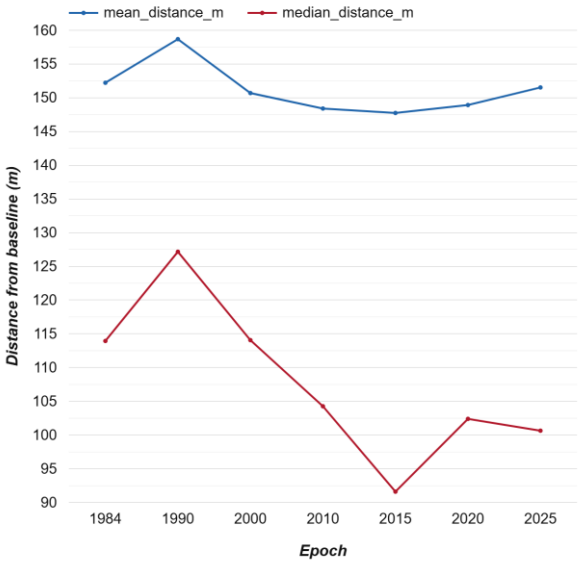


**Figure 7.** Mean and median shoreline distances for the seven primary shoreline epochs used in the 1984-2025 analysis. / **Şekil 7**. 1984-2025 analizinde kullanılan yedi ana kıyı çizgisi dönemi için ortalama ve medyan kıyı çizgisi uzaklıkları.

### 3.2. Period-specific shoreline variability

The period-specific shoreline-change statistics show that Lara Beach did not evolve uniformly over the full study interval. Instead, the record is characterized by alternating positive and negative phases, pointing to repeated shoreline readjustment rather than uninterrupted retreat. As summarized in Table 4, the shoreline advanced during 1984–1990, when mean shoreline position moved seaward by 6.47 m relative to the 1984 baseline condition. This was followed by the strongest retreat phase during 1990–2000, when the mean shoreline position shifted landward by 8.00 m.

Retreat continued during 2000–2010 and 2010–2015, although with lower magnitude than in the preceding interval. After 2015, the pattern changed again. Between 2015 and 2020, mean shoreline position recovered by 1.18 m, and the clearest positive phase occurred during 2020–2025, when recovery reached 2.60 m. The same sequence is also reflected in the year-based shoreline means, which place the lowest average shoreline position in 2015 and the clearest recovery in the two most recent intervals.

An important feature of the period-based results is that the changes in mean shoreline position remain moderate relative to the full alongshore extent of the beach. This indicates that the interval means summarize an aggregate signal rather than a uniform response shared by all sectors. In other words, shoreline change at Lara Beach was not only temporally variable but also spatially uneven, with stronger localized movements exerting greater influence on the interval means.

**Table 4.** Period-specific shoreline change between consecutive primary epochs. / **Tablo 4.** Ardışık birincil dönemler arasındaki dönemsel kıyı çizgisi değişimi.

| Period | Mean NSM (m) | Mean EPR (m/yr) |
|---|---|---|
| 1984-1990 | 6.47 | 1.08 |
| 1990-2000 | -8.00 | -0.80 |
| 2000-2010 | -2.29 | -0.23 |
| 2010-2015 | -0.66 | -0.13 |
| 2015-2020 | 1.18 | 0.24 |
| 2020-2025 | 2.60 | 0.52 |

Overall, the shoreline history of Lara Beach is better described as an oscillatory sequence of advance, retreat, and partial recovery than as a continuously erosional trajectory. At the descriptive level, the post-2015 intervals suggest that at least part of the study reach retained the capacity for partial rebuilding after earlier landward shifts.

### 3.3. Long-term shoreline change metrics and alongshore pattern

The long-term shoreline-change statistics derived from the GEE-based workflow are presented in Table 5. A total of 84 valid transects were retained in the final analysis. Of these, 41 transects (48.81%) were classified as erosional and 43 transects (51.19%) as accretional according to the sign of NSM. The aggregated metrics indicate a negative but small-magnitude long-term tendency, with a mean NSM of -0.69 m, a mean EPR of -0.02 m/yr, and a mean LRR of -0.03 m/yr. Median NSM and median EPR were both 0.00, while

median LRR was likewise centred at 0.00, suggesting that a substantial proportion of the shoreline remained close to relative equilibrium over the 1984-2025 interval.

**Table 5.** Long-term shoreline change metrics derived from the GEE-based analysis. / **Tablo 5.** GEE tabanlı analizden elde edilen uzun dönem kıyı çizgisi değişim metrikleri.

| Metric / Indicator | Value | Unit |
|---|---|---|
| Valid transects | 84 | count |
| Erosion transects | 41 | count |
| Erosion share | 48.81 | % |
| Accretion transects | 43 | count |
| Accretion share | 51.19 | % |
| Mean NSM (1984-2025) | -0.69 | m |
| Median NSM (1984-2025) | 0.00 | m |
| Minimum NSM | -55.24 | m |
| Maximum NSM | 47.68 | m |
| NSM standard deviation | 20.27 | m |
| Mean EPR (1984-2025) | -0.02 | m/yr |
| Median EPR (1984-2025) | 0.00 | m/yr |
| Minimum EPR | -1.35 | m/yr |
| Maximum EPR | 1.16 | m/yr |
| EPR standard deviation | 0.49 | m/yr |
| Mean LRR (1984-2025) | -0.03 | m/yr |
| Median LRR (1984-2025) | 0.00 | m/yr |
| Minimum LRR | -1.23 | m/yr |
| Maximum LRR | 1.33 | m/yr |
| LRR standard deviation | 0.51 | m/yr |

The spatial expression of this long-term variability is shown in Figure 8, which presents the mapped distribution of NSM classes along the study reach. The coastal ribbon indicates that erosional, relatively stable, and accretional parts of the shoreline do not form a simple linear gradient from one end of the beach to the other. Instead, these classes alternate alongshore, indicating a spatially heterogeneous shoreline response within the same coastal setting.

The alongshore expression of this variability is further clarified in Figure 9, which shows the spatial distribution of erosional and accretional transects across the study reach. Rather than forming continuous and clearly separated zones, the two transect classes are interspersed along the shoreline. Although accretional transects slightly outnumber erosional transects, the mean NSM remains negative because retreat is concentrated in fewer transects with stronger landward displacement. Accordingly, the shoreline signal at Lara Beach appears to be shaped less by generalized recession than by the disproportionate influence of localized erosional sectors.

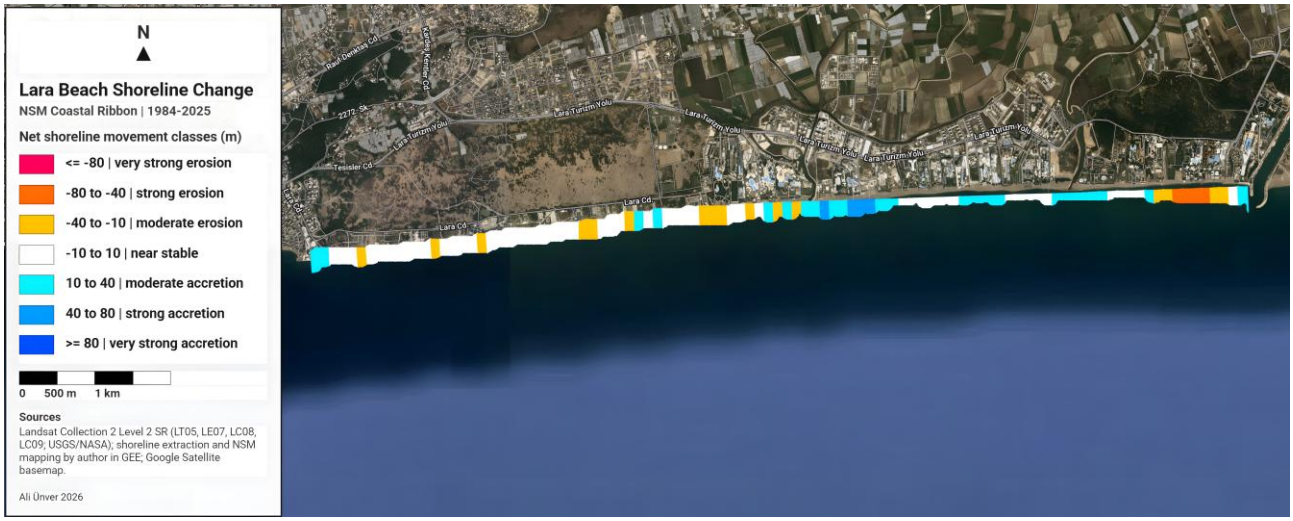


**Figure 8.** NSM-based coastal ribbon showing the sign-based spatial pattern of shoreline retreat, relative stability and seaward advance along Lara Beach. / **Şekil 8.** Lara Plajı boyunca kıyı çizgisi gerilemesi, göreli stabilite ve deniz yönünde ilerleme alanlarının NSM işaretine dayalı mekânsal dağılımını gösteren kıyı şeridi.


**Figure 9.** Spatial distribution of erosion and accretion transects along the study reach. / **Şekil 9.** Çalışma alanı boyunca erozyon ve birikim transektlerinin mekânsal dağılımı.

The statistical distributions of the three principal shoreline-change metrics are shown in Figures 10–12. All three are centred close to zero, consistent with the near-zero median values reported in Table 5. At the same time, the distributions show substantial spread, especially for NSM, indicating that relatively small reach-scale averages conceal considerable transect-scale variability.

Figure 10 shows that NSM values range from −55.24 m to 47.68 m, with a standard deviation of 20.27 m. This wide range indicates that, although the aggregate shoreline tendency is weak, individual transects experienced substantial long-term displacement in both erosional and accretional directions.

The EPR distribution in Figure 11 is likewise centred near zero, but extends from −1.35 m/yr to 1.16 m/yr, with a standard deviation of 0.49 m/yr. These values show that annualized shoreline-change rates varied considerably among transects, even though the long-term mean rate for the study reach remained close to zero.

A similar pattern appears in Figure 12, where LRR values range from −1.23 m/yr to 1.33 m/yr, with a standard deviation of 0.51 m/yr. Because LRR incorporates all primary shoreline epochs rather than only endpoint positions, this distribution further supports the view that shoreline behaviour at Lara Beach was mixed and spatially uneven rather than uniformly erosional.

Taken together, the long-term metrics and their spatial distributions indicate that Lara Beach is characterized by weak aggregate shoreline retreat but pronounced local variability. At the scale of the full study reach, the shoreline appears close to balance while still containing clearly defined sectors of notable erosion and accretion.

**Table 6.** DSAS-derived shoreline change summary metrics. / **Tablo 6.** DSAS tabanlı kıyı çizgisi değişim özet metrikleri.

| Metric | Min | Max | Mean | Median | Std. Dev. | Unit |
|---|---|---|---|---|---|---|
| NSM | -59.86 | 59.85 | -3.08 | 0.00 | 24.15 | m |
| EPR | -2.30 | 5.98 | 0.00 | 0.00 | 1.12 | m/yr |
| LRR | -2.29 | 5.98 | -0.01 | -0.01 | 1.09 | m/yr |
| SCE | 0.00 | 59.88 | 26.41 | 29.93 | 20.87 | m |

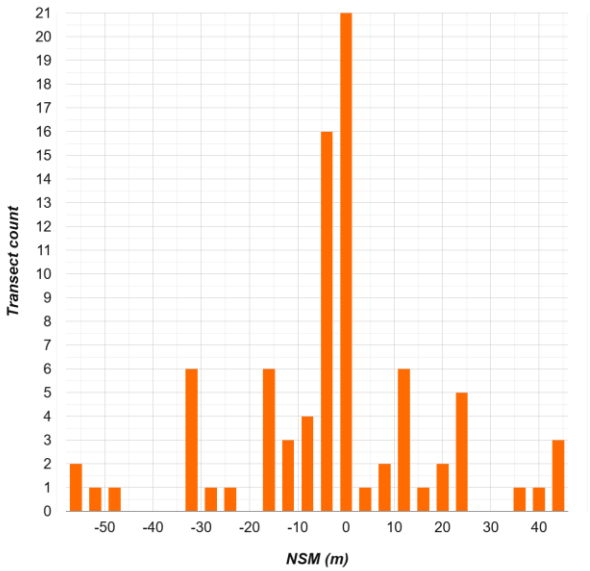


**Figure 10.** Distribution of NSM values across valid transects. / **Şekil 10.** Geçerli transektler boyunca NSM değerlerinin dağılımı.

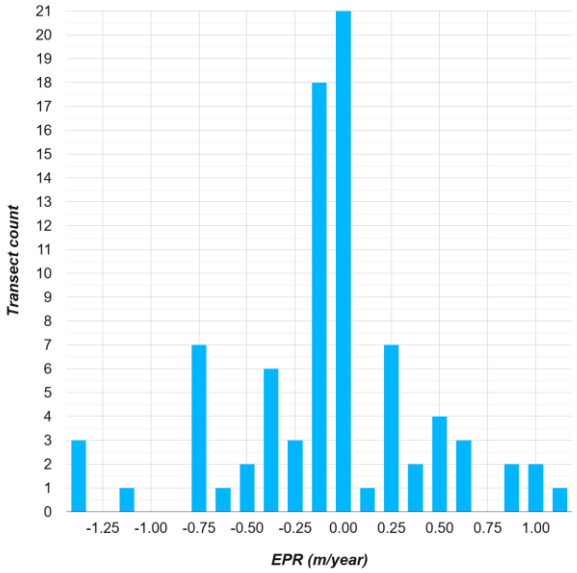


**Figure 11.** Distribution of EPR values across valid transects. / **Şekil 11.** Geçerli transektler boyunca EPR değerlerinin dağılımı.

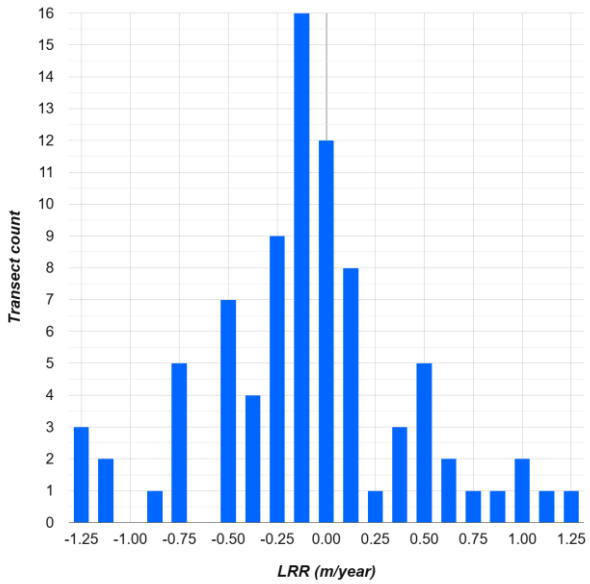


**Figure 12.** Distribution of LRR values across valid transects. / **Şekil 12.** Geçerli transektler boyunca LRR değerlerinin dağılımı.

### 3.4. DSAS-based comparison and cross-platform consistency

The shoreline-change results derived from the GEE-based workflow were compared with DSAS outputs in order to assess cross-platform consistency. Summary statistics for the DSAS-derived metrics are presented in Table 6. For the matched transects, mean NSM was −3.08 m, mean EPR was 0.00 m/yr, and mean LRR was −0.01 m/yr. The DSAS dataset also yielded a mean SCE of 26.41 m, indicating a moderate shoreline-envelope width across the analysed transects. Only transects that produced one-to-one valid results in both workflows were retained for direct comparison, which reduced the comparison subset to 66 matched transects. The broad NSM range in the DSAS dataset, extending from −59.86 m to 59.85 m, supports

the same general descriptive interpretation obtained from the GEE analysis: Lara Beach displays mixed long-term shoreline behaviour with substantial local variability.

The mean SCE value of 26.41 m is also important for interpreting shoreline mobility at Lara Beach. Although the long-term directional metrics indicate weak aggregate retreat at the reach scale, SCE shows that several transects experienced a relatively wide envelope of shoreline movement between the analysed epochs. This means that a transect with limited final 1984–2025 displacement may still have undergone marked intermediate shoreline shifts. In this sense, SCE complements NSM, EPR and LRR by identifying sectors where shoreline mobility is high even when the net long-term direction is weak. From a coastal-management perspective, such sectors require attention because repeated landward and seaward shoreline movements may affect beach width, recreational use, foreshore stability and the planning of monitoring priorities.

The alongshore comparison between GEE- and DSAS-derived NSM values is shown in Figure 13. The two analytical approaches reproduce a broadly similar spatial pattern along the study reach, even though they do not coincide exactly at every transect. Agreement is particularly clear in sectors showing marked positive or negative departures from zero, whereas the largest discrepancies are concentrated in a relatively limited number of transects. Overall, the alongshore comparison indicates that both approaches capture the same dominant spatial structure of shoreline change, despite local differences in magnitude.

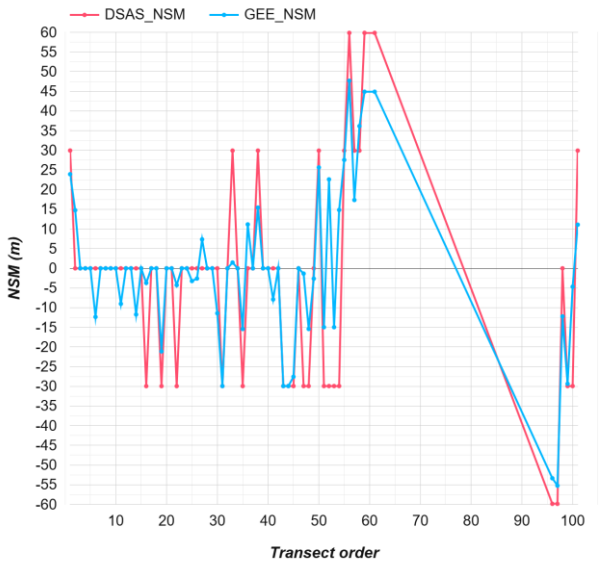


**Figure 13.** Alongshore comparison of NSM values derived from GEE and DSAS. / **Şekil 13.** GEE ve DSAS'tan türetilen NSM değerlerinin kıyı boyunca karşılaştırılması.

A statistical comparison of the matched transects is summarized in Table 7 and illustrated in Figures 14–16. For NSM, the correlation between GEE and DSAS is strong ($r$ = 0.838) across 66 matched transect pairs, with a mean absolute difference of 7.98 m and a mean bias of −1.851 m (DSAS minus GEE). For EPR, the correlation remains substantial ($r$ = 0.779), while the mean absolute difference decreases to 0.348 m/yr and the mean bias to 0.049 m/yr. LRR shows the lowest, though still meaningful, level of agreement ($r$ = 0.733), with a mean absolute difference of 0.341 m/yr and a mean bias of 0.041 m/yr. These results indicate that the GEE-based workflow reproduces the principal statistical structure of shoreline change identified by DSAS, even though some local deviations remain.

**Table 7.** Summary of agreement between GEE- and DSAS-derived shoreline change metrics. / **Tablo 7.** GEE ve DSAS'tan türetilen kıyı çizgisi değişim metrikleri arasındaki uyumun özeti.

| Metric | Matched pairs | Pearson r | Mean absolute difference | Median absolute difference | Maximum absolute difference | Mean bias (DSAS – GEE) | Unit |
|---|---|---|---|---|---|---|---|
| NSM | 66 | 0.838 | 7.980 | 2.919 | 52.536 | -1.851 | m |
| EPR | 66 | 0.779 | 0.348 | 0.069 | 4.890 | 0.049 | m/yr |
| LRR | 66 | 0.733 | 0.341 | 0.147 | 5.191 | 0.041 | m/yr |

The scatter relationship for NSM is presented in Figure 14. The positive linear association between the two datasets shows that transects identified by DSAS as more strongly erosional or more strongly accretional generally occupy comparable positions in the GEE results.

Although there is visible dispersion around the fitted relationship, the overall trend remains clear.

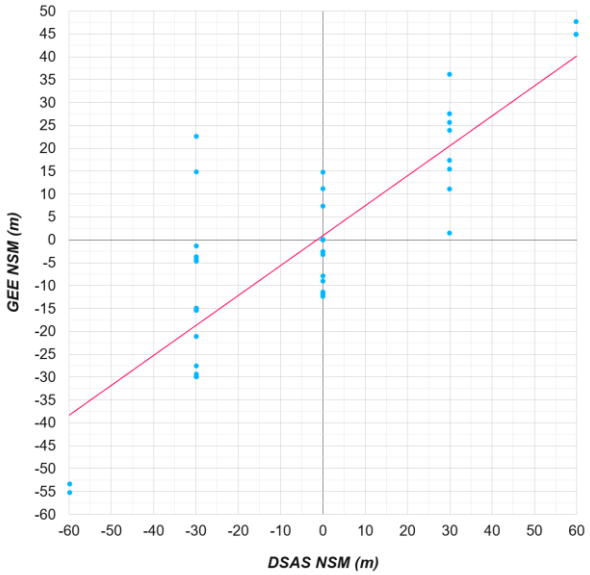


**Figure 14.** Scatter comparison of NSM values derived from GEE and DSAS for matched transects. / **Şekil 14.** Eşleştirilmiş transektler için GEE ve DSAS'tan türetilen NSM değerlerinin saçılım karşılaştırması.

A similar pattern is observed for EPR in Figure 15. Although some spread is present, the data still show a clear positive association, indicating that both methods identify broadly comparable annualized shoreline-change tendencies at the transect scale.

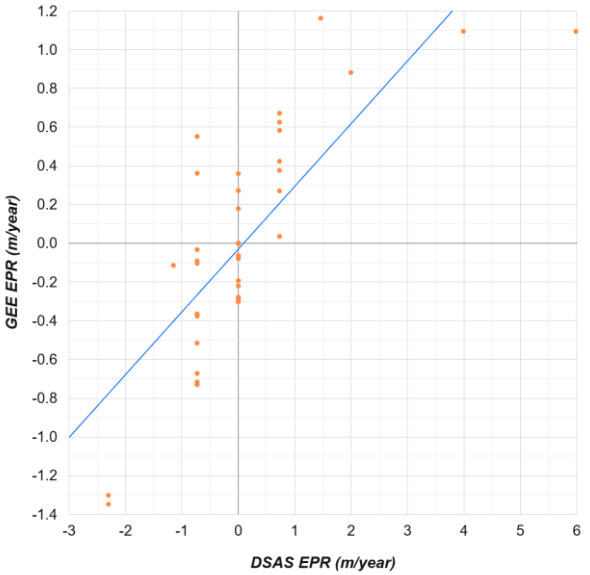


**Figure 15.** Scatter comparison of EPR values derived from GEE and DSAS for matched transects. / **Şekil 15.** Eşleştirilmiş transektler için GEE ve DSAS'tan türetilen EPR değerlerinin saçılım karşılaştırması.

The relationship for LRR is shown in Figure 16. Compared with NSM and EPR, the agreement is somewhat weaker, which is consistent with the lower correlation coefficient reported in Table 7. Even so, the scatter still indicates a meaningful positive association between the two approaches. Because LRR incorporates all valid shoreline epochs rather than only endpoint conditions, small methodological differences in shoreline positioning and transect-intersection handling are more likely to affect this metric. Nevertheless, the overall correspondence remains sufficiently strong to support the reliability of the GEE-based shoreline-change framework.

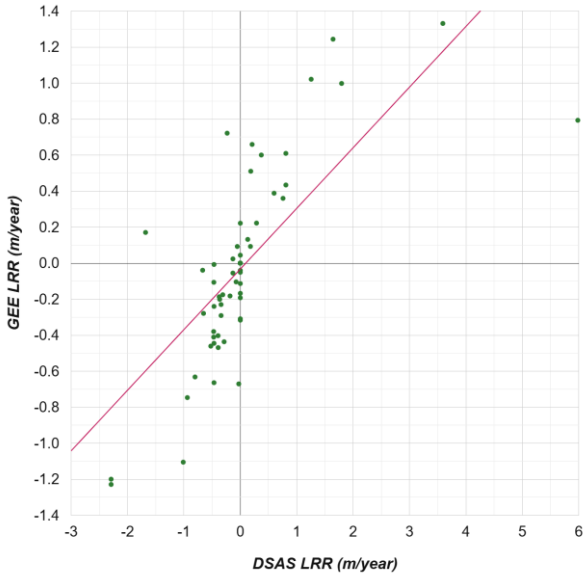


**Figure 16.** Scatter comparison of LRR values derived from GEE and DSAS for matched transects. / **Şekil 16.** Eşleştirilmiş transektler için GEE ve DSAS'tan türetilen LRR değerlerinin saçılım karşılaştırması.

Overall, the comparison shows that the GEE-based workflow and DSAS converge on the same broad interpretation of shoreline behaviour at Lara Beach: weak aggregate retreat at the reach scale, substantial local variability, and a mixed spatial structure of erosion and accretion. This agreement increases confidence in the robustness of the multi-decadal shoreline reconstruction used in the present study.

### 3.5. Field observations supporting shoreline-change interpretation

Field observations provide a present-day geomorphological context for selected parts of the Lara Beach study reach (Figure 17). The photographic record shows laterally continuous sandy foreshore surfaces in some parts of the beach, while the stream/channel-mouth area displays a more complex setting with artificial

margins, low-gradient water-edge conditions and local sediment accumulation. These observations help interpret the current expression of the mapped shoreline-change sectors, but they do not verify the historical GEE or DSAS shoreline positions.

The stream/channel-mouth sector is especially important for interpretation because it combines marine influence with local sediment storage and human-modified boundaries. In this part of the coast, sediment accumulation near the channel margins and artificial rock boundaries may affect the short-term position of the land-water boundary. This supports a cautious, sector-based interpretation of the shoreline-change pattern.

The presence of stockpiled sediment and machinery near the beach/channel-mouth sector was recorded as evidence of local sediment handling or possible reworking. It is not treated as proof of systematic beach nourishment, because the study does not include operational records or repeated field monitoring of sediment movement.


**Figure 17.** Contemporary field photographs showing present-day geomorphological and human-modified coastal conditions at Lara Beach: (a-b) sandy foreshore and upper-beach sectors; (c-d) stream/channel-mouth margins with local sediment accumulation and artificial boundaries; (e) stockpiled sediment and machinery near the beach/channel-mouth area; (f) upstream channel reach with landscaped or artificial margins. The photographs are used as interpretive field support rather than as direct validation of the historical shoreline positions. / **Şekil 17.** Lara Plajı'nda güncel jeomorfolojik koşulları ve insan etkisiyle değişmiş kıyı ortamlarını gösteren saha fotoğrafları: (a-b) kumlu kıyı önü ve üst plaj kesimleri; (c-d) yerel sediman birikimi ve yapay sınırların izlendiği akarsu/kanal ağzı kenarları; (e) plaj/kanal ağzı yakınında istiflenmiş sediman ve iş makinesi; (f) peyzajlı veya yapay kenarlara sahip kanalın yukarı kesimi. Fotoğraflar, tarihsel kıyı çizgisi konumlarının doğrudan doğrulanması için değil, güncel jeomorfolojik yorum desteği olarak kullanılmıştır.

## 4. DISCUSSION

### 4.1. Interpreting the long-term behaviour of Lara Beach

The long-term shoreline record at Lara Beach is best read from the site's own metrics before comparison with other coasts. The GEE-derived mean values are negative, but their magnitude is small, and the transect counts show 41 erosional and 43 accretional transects. The main result is therefore not only the sign of the reach-scale mean, but the coexistence of retreating and advancing sectors within the same 10.12 km sandy beach reach.

Recent Turkish studies are used here as methodological and conceptual context, not as independent validation of the Lara findings. The interpretation of Lara Beach rests on its own

NSM, EPR and LRR values, spatial shoreline-change maps, GEE-DSAS comparison and present-day field observations. The wider literature mainly shows why a single average rate can be misleading in Turkish coastal settings and why sector-based interpretation is necessary (Uzun, 2023; Öztürk & Uzun, 2023; Kılar & Aydın, 2024; Kılar & Kömüşcü, 2024; Öztürk & Maraş, 2024; Öztürk & Sesli, 2015; Öztürk et al., 2015; Ateş et al., 2024; Uzun, 2024; Uzun, 2025).

The temporal sequence also comes from the Lara data themselves. The shoreline advanced during 1984-1990, retreated more clearly through the middle of the record, and showed partial recovery after 2015. This pattern suggests alternating shoreline adjustment rather than continuous retreat. The scope of the present study is to quantify and map shoreline-position change using Landsat-GEE and DSAS; it does not present a new sediment budget, hydrodynamic model, wave-current analysis or repeated field survey. Possible controls are therefore discussed as interpretive factors and future research needs, not as demonstrated process mechanisms.

### 4.2. Alongshore heterogeneity and geomorphological controls

One of the clearest outcomes of the study is the alongshore differentiation of shoreline change. The NSM coastal ribbon, the erosion-accretion transect map and the metric distributions show that retreating, near-stable and advancing transects alternate along the beach rather than forming a single uniform gradient. This spatial pattern is especially relevant because Lara includes a stream/channel-mouth sector, artificial margins, constrained backshore zones and locally variable foreshore widths.

Several local controls may help explain this heterogeneity, although the available data do not prove a single causal pathway. The observed alternation between erosional and accretional transects should therefore be interpreted as the geomorphic expression of a locally variable sediment-exchange system rather than as a uniform shoreline translation. In sandy Mediterranean coastal settings, shoreline position may respond to wave energy, storm-driven swash processes, alongshore sediment redistribution, seasonal beach recovery, sediment supply, and the degree of backshore accommodation space (Carter, 1988; Komar, 1998; Masselink & Hughes, 2003; Boak & Turner, 2005).

At Lara Beach, the stream/channel-mouth sector may act as a local sediment-storage and reworking zone. In this part of the coast, the position of the mapped land-water boundary may be affected by short-term sediment accumulation, channel-mouth morphology and artificial margins. By contrast, sectors with constrained backshore conditions or human-modified boundaries may have lower capacity for landward adjustment during erosional phases. These local differences help explain why neighbouring transects may show retreat, relative stability or seaward advance within the same overall beach system.

The negative reach-scale mean should therefore not be interpreted as evidence of uniform and continuous erosion along the entire Lara Beach shoreline. Instead, it reflects the balance between numerous small positive or near-stable changes and a smaller number of stronger retreating transects. This pattern indicates that shoreline change is controlled by sector-specific geomorphological conditions rather than by a single process acting equally along the whole coast.

The field photographs support this sector-based interpretation. They show wider sandy foreshore surfaces in some parts of the beach, local sediment accumulation near the stream/channel-mouth area, and artificial or landscaped margins in adjacent backshore/channel settings. These observations suggest that present-day shoreline behaviour is locally conditioned by sediment storage, foreshore width, backshore constraint and anthropogenic modification. However, because the study does not include hydrodynamic modelling, sediment-budget analysis or repeated field surveys, these controls are interpreted as plausible geomorphological explanations rather than as directly measured process mechanisms.

Overall, the shoreline-change pattern at Lara Beach is best understood as the product of interaction between natural coastal dynamics and human-modified boundary conditions. This interpretation links the GEE and DSAS results

with possible coastal processes, local sediment behaviour and management-relevant shoreline mobility, and therefore gives the mapped erosion-accretion pattern a clearer geomorphological meaning.

### 4.3. Cross-platform consistency and methodological implications

The comparison with DSAS provides a quantitative check on the GEE workflow. Across 66 matched transects, the correlation values are 0.838 for NSM, 0.779 for EPR and 0.733 for LRR. Mean absolute differences are 7.98 m for NSM, 0.348 m/yr for EPR and 0.341 m/yr for LRR. These values show that the two workflows reproduce the same main shoreline pattern, although they should not be expected to match exactly at every transect.

SCE adds a further check in the DSAS output by showing the width of the shoreline-change envelope. Although it does not indicate whether the shoreline ultimately retreated or advanced, it provides important information on the maximum spatial range of shoreline movement along each transect. For this reason, SCE is interpreted here as a complementary mobility indicator rather than as a directional trend metric. This distinction is important for Lara Beach because sectors with near-zero NSM or EPR values may still have experienced considerable intermediate shoreline movement. Therefore, SCE helps identify parts of the coast where shoreline mobility may be relevant for future monitoring and coastal-management decisions.

The agreement is important because both workflows identify the same broad pattern: a small negative reach-scale mean together with pronounced local variability. Differences at individual transects are expected because GEE and DSAS differ in shoreline extraction, geometry handling and intersection rules. These differences should not be read as a failure of either method; they define the uncertainty envelope within which the results should be interpreted.

Methodologically, the study shows that a GEE workflow can be useful for long-term shoreline monitoring when its limits are stated clearly. The strength of GEE in this work is the ability to process long Landsat archives consistently and to repeat the workflow transparently. Its limitation is that medium-resolution optical imagery still requires careful interpretation, especially on sandy beaches where wet sand, swash conditions and seasonal morphology can influence the extracted shoreline proxy. Comparable DSAS-based applications also emphasize that method-related differences should be evaluated through overall spatial tendency and uncertainty, rather than exact transect-by-transect equivalence (Abd-Elhamid et al., 2023; Hossen & Sultana, 2023).

### 4.4. Implications for coastal management and future work

From a coastal-management perspective, Lara Beach should not be evaluated through a single average erosion rate. The mean values are useful as summary indicators, but they do not adequately represent the spatially variable shoreline behaviour identified in this study. Management attention should focus on sectors where stronger shoreline retreat occurs, where SCE values indicate a wider shoreline-mobility envelope, where artificial boundaries constrain the backshore, and where the stream/channel-mouth sector stores or reworks sediment.

A dedicated monitoring strategy should therefore be sector-based and spatially explicit. Repeated shoreline mapping should be combined with field-based beach-width measurements, berm and scarp observations, post-storm checks and targeted monitoring of the stream/channel-mouth area. This would help distinguish temporary shoreline oscillation from persistent erosional tendency and would provide a stronger basis for beach-use planning, tourism infrastructure management and erosion-risk reduction.

The findings also have implications for future shoreline change under continued coastal use and potential increases in storm impact or sea-level-related shoreline pressure. Sectors with high mobility or localized retreat may become more sensitive if backshore accommodation space is limited by infrastructure or artificial margins. Therefore, future management should avoid interpreting the beach as a uniform geomorphic unit and should instead prioritize the identification of local erosion hotspots, mobile sediment-storage areas and constrained foreshore/backshore transitions.

The present study does not claim to have resolved the full process history of Lara Beach. Seasonal shoreline positions, storm chronology, sediment pathways, engineering influence and backshore constraint should be tested with higher-resolution imagery, repeated field surveys and, where possible, sediment-budget or hydrodynamic data. A denser transect network, for example 30–50 m spacing, could also improve the detection of local shoreline responses. However, applying such a network would require complete reprocessing of both GEE and DSAS outputs; therefore, the 100 m transect framework used here is retained as an internally consistent basis for the present multi-decadal comparison.

## 5. CONCLUSIONS

This study quantified shoreline change along Lara Beach for the 1984-2025 period using Landsat-derived shorelines processed in GEE, transect-based NSM, EPR and LRR metrics, and a comparison with DSAS. The analysis shows that Lara Beach cannot be described as a uniformly retreating shoreline. The reach-scale mean is negative, but the magnitude is small and the transect-level results show both erosion and accretion along the same beach.

The GEE results indicate mean NSM of -0.69 m, mean EPR of -0.02 m/yr and mean LRR of -0.03 m/yr. Of the 84 valid transects, 41 are erosional and 43 are accretional. This distribution indicates that the overall negative mean is produced by localized stronger retreat rather than by a uniform landward movement of the entire shoreline.

The temporal pattern is oscillatory. The shoreline advanced in 1984-1990, retreated more clearly between 1990 and 2015, and showed partial recovery after 2015. These results indicate repeated shoreline adjustment through time and support a sector-based interpretation of Lara Beach.

The DSAS comparison supports the reliability of the main pattern. Correlations of 0.838 for NSM, 0.779 for EPR and 0.733 for LRR indicate that GEE and DSAS reproduce the same broad spatial structure, even though individual transects differ because of workflow and geometry-related factors.

In management terms, Lara Beach should be monitored by sectors rather than through a single reach-wide average. Priority should be given to localized erosion zones, sectors with wider SCE-defined shoreline-mobility envelopes, the stream/channel-mouth sector, and parts of the beach where artificial boundaries or backshore constraint may affect foreshore adjustment. Future monitoring should combine repeated satellite mapping with beach-width measurements, berm/scarp observations, post-storm field checks and sediment observations.

The 100 m transect spacing used in this study provides an internally consistent framework for the multi-decadal GEE–DSAS comparison, but it may smooth very local shoreline responses. Future studies could improve the spatial resolution of the analysis by applying a denser transect network, higher-resolution imagery, seasonal shoreline comparisons and repeated field measurements. Such work would help test the process-based interpretations proposed here, especially around the stream/channel-mouth sector and other locally mobile parts of Lara Beach.

## REFERENCES

Abd-Elhamid, H. F., Zelenakova, M., Baranczuk, J., Bindzarova Gergelova, M., & Mahdy, M. (2023). Historical trend analysis and forecasting of shoreline change at the Nile Delta using RS data and GIS with the DSAS tool. Remote Sensing, 15(7), 1737. https://doi.org/10.3390/rs15071737

Akdeniz, H. B., & İnam, Ş. (2023). Spatio-temporal analysis of shoreline changes and future forecasting: The case of Küçük Menderes Delta, Türkiye. Journal of Coastal Conservation, 27, 34. https://doi.org/10.1007/s11852-023-00966-8

Ateş, E., Gül, M., Sarıman, G., & Danladi, I. B. (2024). Akarsular üzerindeki antropojenik yapıların kıyı çizgisi üzerindeki etkisi: Dalaman Çayı. Geomatik, 9(2), 245-258. https://doi.org/10.29128/geomatik.1434927

Ataol, M., Kale, M. M., & Tekkanat, İ. S. (2019). Assessment of the changes in shoreline using digital shoreline analysis system: A

case study of Kızılırmak Delta in northern Turkey from 1951 to 2017. Environmental Earth Sciences, 78, 579. https://doi.org/10.1007/s12665-019-8591-7

Boak, E. H., & Turner, I. L. (2005). Shoreline definition and detection: A review. Journal of Coastal Research, 21(4), 688-703. https://doi.org/10.2112/03-0071.1

Carter, R. W. G. (1988). Coastal environments: An introduction to the physical, ecological and cultural systems of coastlines. Academic Press.

Ciritci, D., & Türk, T. (2020). Analysis of coastal changes using remote sensing and geographical information systems in the Gulf of İzmit, Turkey. Environmental Monitoring and Assessment, 192, 341. https://doi.org/10.1007/s10661-020-08255-9

Crowell, M., Leatherman, S. P., & Buckley, M. K. (1991). Historical shoreline change: Error analysis and mapping accuracy. Journal of Coastal Research, 7(3), 839-852. https://journals.flvc.org/jcr/article/view/78539

Darwish, K., & Smith, S. (2023). Landsat-based assessment of morphological changes along the Sinai Mediterranean coast between 1990 and 2020. Remote Sensing, 15(5), 1392. https://doi.org/10.3390/rs15051392

Gorelick, N., Hancher, M., Dixon, M., Ilyushchenko, S., Thau, D., & Moore, R. (2017). Google Earth Engine: Planetary-scale geospatial analysis for everyone. Remote Sensing of Environment, 202, 18-27. https://doi.org/10.1016/j.rse.2017.06.031

Gümüş, M. G. (2024). Forecasting future scenarios of coastline changes in Türkiye's Seyhan Basin: A comparative analysis of statistical methods and Kalman Filtering (2033-2043). Earth Science Informatics, 17, 5207-5232. https://doi.org/10.1007/s12145-024-01445-w

Himmelstoss, E. A., Henderson, R. E., Kratzmann, M. G., & Farris, A. S. (2021). Digital Shoreline Analysis System (DSAS) version 5.1 user guide (U.S. Geological Survey Open-File Report 2021-1091). U.S. Geological Survey. https://doi.org/10.3133/ofr20211091

Hossen, M. F., & Sultana, N. (2023). Shoreline change detection using DSAS technique: Case of Saint Martin Island, Bangladesh. Remote Sensing Applications: Society and Environment, 30, 100943. https://doi.org/10.1016/j.rsase.2023.100943

Kale, M. M., Ataol, M., & Tekkanat, İ. S. (2019). Assessment of shoreline alterations using a Digital Shoreline Analysis System: A case study of changes in the Yeşilırmak Delta in northern Turkey from 1953 to 2017. Environmental Monitoring and Assessment, 191, 398. https://doi.org/10.1007/s10661-019-7535-8

Kılar, H. (2023). Shoreline change assessment using DSAS technique: A case study on the coast of Meriç Delta (NW Türkiye). Regional Studies in Marine Science, 57, 102737. https://doi.org/10.1016/j.rsma.2022.102737

Kılar, H., & Aydın, O. (2024). Temporal shoreline changes from 1984 to 2022 along Beymelek Beach and Beymelek Lagoon, Antalya, Türkiye. Jeomorfolojik Araştırmalar Dergisi, 13, 40-51. https://doi.org/10.46453/jader.1497770

Kılar, H., & Çiçek, İ. (2018). Göksu Deltası kıyı çizgisi değişiminin DSAS aracı ile belirlenmesi. Coğrafi Bilimler Dergisi, 16(1), 89-104. https://doi.org/10.1501/Cogbil_0000000192

Kılar, H., & Kömüşcü, A. Ü. (2024). Temporal analysis of the coastal erosion and accretion on the shoreline of Bakırçay Delta of Türkiye by Digital Shoreline Analysis System (DSAS). International Journal of Environment and Geoinformatics, 11(4), 47-57. https://doi.org/10.26650/ijegeo.1467190

Komar, P. D. (1998). Beach processes and sedimentation (2nd ed.). Prentice Hall.

Kuleli, T. (2010). Quantitative analysis of shoreline changes at the Mediterranean coast in Turkey. Environmental Monitoring and Assessment, 167(1-4), 387-397. https://doi.org/10.1007/s10661-009-1057-8

Masselink, G., & Hughes, M. G. (2003). Introduction to coastal processes and geomorphology. Arnold.

Molina, R., Anfuso, G., González-Aguilar, B., Manno, G., & Cooper, J. A. G. (2024). Evolution of the beach-dune systems in Mediterranean Andalusia (Spain) using two different proxies. Land, 13(8), 1185. https://doi.org/10.3390/land13081185

Özpolat, E., & Demir, T. (2019). The spatiotemporal shoreline dynamics of a delta under natural and anthropogenic conditions from 1950 to 2018: A dramatic case from the Eastern Mediterranean. Ocean & Coastal Management, 180, 104910. https://doi.org/10.1016/j.ocecoaman.2019.104910

Özpolat, E., Şahiner, E., Özcan, O., Demir, T., & Owen, L. A. (2021). Late-Holocene landscape evolution of a delta from foredune ridges: Seyhan Delta, Eastern Mediterranean, Turkey. The Holocene, 31(5), 760-777. https://doi.org/10.1177/0959683620988047

Öztürk, D., & Maraş, E. E. (2024). Investigation of the effects of small fishing ports on the shoreline: A case study of Samsun, Turkey. Journal of Coastal Conservation, 28, 20. https://doi.org/10.1007/s11852-023-01012-3

Öztürk, D., & Sesli, F. A. (2015). Shoreline change analysis of the Kızılırmak Lagoon Series. Ocean & Coastal Management, 118, 290-308. https://doi.org/10.1016/j.ocecoaman.2015.03.009

Öztürk, D., & Uzun, S. (2023). Kızılırmak Deltası kıyı çizgisinin EPR ve LRR yöntemleriyle 1984-2022 periyodunda değişim analizi ve 2030 yılı tahmini. Coğrafi Bilimler Dergisi, 21(2), 306-339. https://doi.org/10.33688/aucbd.1310132

Öztürk, D., Beyazıt, İ., & Kılıç Gül, F. (2015). Spatiotemporal analysis of shoreline changes of the Kızılırmak Delta. Journal of Coastal Research, 31(6), 1389-1402. https://doi.org/10.2112/JCOASTRES-D-14-00159.1

Thieler, E. R., Himmelstoss, E. A., Zichichi, J. L., & Ergul, A. (2009). Digital Shoreline Analysis System (DSAS) version 4.0: An ArcGIS extension for calculating shoreline change (U.S. Geological Survey Open-File Report 2008-1278). U.S. Geological Survey. https://doi.org/10.3133/ofr20081278

Uzun, M. (2023). Riva (İstanbul) kıyılarında doğal ve antropojenik etkenlerle değişen kıyı çizgisinin DSAS aracı ile analizi. Jeomorfolojik Araştırmalar Dergisi, 11, 95-113. https://doi.org/10.46453/jader.1335105

Uzun, M. (2024). İzmit Körfezi doğu kıyısındaki doğal ve antropojenik kökenli değişimlerin DSAS aracı ile analizi. Turkish Journal of Remote Sensing and GIS, 5(1), 83-101. https://doi.org/10.48123/rsgis.1410923

Uzun, M. (2025). Karaburun-Kumköy (İstanbul) arası kıyı şeridinde meydana gelen değişimlerin DSAS aracı ile antropo-jeomorfolojik analizi. Jeomorfolojik Araştırmalar Dergisi, 14, 48-73. https://doi.org/10.46453/jader.1621372

Xu, H. (2006). Modification of normalised difference water index (NDWI) to enhance open water features in remotely sensed imagery. International Journal of Remote Sensing, 27(14), 3025-3033. https://doi.org/10.1080/01431160600589179